MOLECULAR SIMULATION
2020, VOL. 46, NO. 1, 33–40
https://doi.org/10.1080/08927022.2019.1667498

Taylor & Francis
Taylor & Francis Group

Check for updates

Directed transport of liquid droplets on vibrating substrates with asymmetric corrugations and patterned wettability: a dissipative particle dynamics study

Xinran Geng[a], Xiaopeng Yu[a], Luyao Bao[b], Nikolai V. Priezjev[c] and Yang Lu[a]

[a]Jilin Provincial Key Laboratory for Numerical Simulation, Jilin Normal University, Siping, People's Republic of China; [b]School of Marine Science and Technology, Northwestern Polytechnical University, Xi'an, People's Republic of China; [c]Department of Mechanical and Materials Engineering, Wright State University, Dayton, OH, USA

ABSTRACT

The development of digital (droplet-based) microfluidic (DMF) devices has received significant attention due to their importance for chemical and biomedical analyses. The precise control and manipulation of liquid droplets on a solid substrate is a major requirement for DMF devices. In this study, we propose a novel strategy to generate continuous droplet motion by combining asymmetric corrugations and patterned wettability on a vibrating substrate. The time periodic oscillations of the substrate with asymmetric triangle corrugations provide the input energy to transport a droplet along patterned stripes. Using dissipative particle dynamic (DPD) simulations, we demonstrate that hydrophobic stripes on a superhydrophobic substrate create a wettability step, which effectively constrains the droplet motion along the stripe. Due to the special design of asymmetric triangle corrugations and orientation of hydrophobic stripes, the proposed strategy enables the transport of multiple droplets with different initial locations towards a single spot and coalescence into a large droplet. We further identify a power-law dependence between the droplet velocity and the period of substrate vibration and show that this function is independent of the droplet size. The proposed droplet transportation strategy can be potentially useful for the efficient manipulation of liquid droplets in DMF devices.

ARTICLE HISTORY
Received 11 June 2019
Accepted 30 August 2019

KEYWORDS
Droplet transport; wettability step; substrate vibration; dissipative particle dynamic simulations

1. Introduction

Microfluidic systems involve operation of small volumes of fluids and can vastly reduce the space and time required for chemical and biological analyses in numerous applications [1]. Droplets, the most common form of small-volume fluid, serve as a straightforward choice of working medium for microfluidic systems. Digital (droplet-based) microfluidic (DMF) devices are in the centre of the intensive research and development of separation and extraction processes. The successful operation of DMF devices relies on a thorough understanding and precise control of the droplet transport [2]. During the past decades, various methods have been proposed for the directed transport of liquid droplets. In particular, the electrowetting on dielectric substrates (EWOD) is self-contained, i.e. it requires no moving parts or fixed channels, and, thus, it is a feasible method to manipulate droplets in DMF [2]. EWOD has been successfully applied for the droplet transport [3–5], merging [6–8], mixing [9,10] and splitting [11]. However, a common problem encountered in EWOD is the so-called electrical breakdown [12,13], which leads to the failure of EWOD.

Due to the spatial variation of the capillary force [14], temperature [15–17] or wettability [10,18–20] gradients applied along the substrate can also induce droplet motion along a preferred direction. Recently, the manipulation of liquid droplets, using substrate vibration, attracted increased attention due to the relatively simple set-up and high process flexibility [10,18,19]. One of the major advantages of the droplet motion induced by substrate vibration is that droplets can be continuously transported over long distances [21]. Another natural advantage of droplet transportation, using substrate vibration, is the enhancement of mixing between two coalescing droplets. Recent studies [8,9,22] showed that the substrate vibration can significantly enhance the mixing rate of two fusing droplets. Previous studies [21] have also demonstrated that the velocity of transported droplets induced by substrate vibration is size dependent, which leads to the application of sorting droplets based on their sizes. Although experiments and simulations have shown the potential for droplet transportation using substrate vibration, the direction of droplet motion remained uncontrollable in previous studies. For example, in the previous study by Tretyakov and Müller [21] using molecular dynamic simulations, a cylindrical droplet, or a ridge, was considered and the droplet was shown to move only in one direction, i.e. the direction perpendicular to the axis of the cylinder. In the case of a three-dimensional spherical droplet residing on an asymmetric corrugated substrate, the droplet moves irregularly on the substrate. Despite extensive efforts, a method for directionally controllable droplet transport using substrate vibration is still lacking.

In this work, we propose a novel strategy to transport liquid droplets along a specified direction on a vibrating substrate patterned with asymmetric corrugations and a wettability step. The triangular corrugation of the vibrated substrate provides an input energy to transport the droplet. In addition, the wettability step, introduced by patterning the superhydrophobic

CONTACT Xiaopeng Yu yyxxpp@jlnu.edu.cn
© 2019 Informa UK Limited, trading as Taylor & Francis Group

substrate with a hydrophobic stripe, is used to control the direction of droplet motion, which is determined by the orientation of the hydrophobic stripe. Adopting the proposed strategy, we demonstrate that multiple droplets with different initial locations can be transported towards a single spot along the intersecting hydrophobic strips using many-body dissipative particle dynamic (DPD) simulations. Furthermore, the dependence of droplet velocity on the period of substrate vibration, droplet size, and stripe width is examined. It will be shown that the droplet velocity increases with decreasing vibration period, but it is independent of the droplet size. We identify a power-law dependence between the droplet velocity and period of substrate vibration. Moreover, we show that different orientations of the hydrophobic stripe do not significantly influence the droplet motion. The results obtained in this work pave the way for design of the droplet transport methods using substrate vibration in DMF devices.

2. Simulation methods

The typical size of liquid droplets in DMF is less than 1 μL; thus, the motion is difficult to measure experimentally. Alternatively, various simulation methods were widely used to study the dynamics and statics of droplets in contact with chemically heterogeneous or corrugated substrates, for example, molecular dynamic simulations [23–29] and continuum fluid mechanic simulations [30,31]. Atomistic simulations can resolve the fluid dynamics at the atomic level, but the time and length scales are restricted to at most tens of nanometres and nanoseconds, respectively. In the opposite limit, continuum models can address problems on larger time and length scales. However, a common difficulty encountered in the continuum approach is the stress singularity at the three-phase contact line of a liquid droplet in contact with a solid surface [32,33]. Moreover, it is difficult for grid-based Navier–Stokes solvers to directly use the interface-tracking algorithms [34].

For the specific problem considered in the present study, only mesoscopic structures of molecules and their collective behaviour are of particular interest. Therefore, coarse-grained (CG) simulation models can be used as an efficient simulation tool to capture the correct dynamics of fluid on large spatial and temporal scales, beyond the capability of conventional atomistic simulations [35,36]. CG simulations drastically simplify the atomistic dynamics by eliminating fast degrees of freedom, while retaining a coarse particle-based description. A single CG particle represents an entire cluster of atoms. In addition, CG interactions also have soft interaction potentials, allowing for larger integration time steps. In comparison with continuum models, CG simulations are grid-free and particle-based, thus naturally avoiding the stress singularity at the three-phase contact line [34]. The many-body DPD [37] is one of the most popular CG methods successfully used to investigate the droplet behaviour on solid substrates [38–43].

Table 1. The parameters in DPD units used in the present study.

Parameters	Symbol	Value
Particle density	ρ	6.00
Cut-off radius of attractive force	r_c	1.00
Cut-off radius of repulsive force	r_d	0.75
Time step	Δt	0.01
System temperature	k_BT	1.00
Amplitude of white noise	δ	6.00
Attraction parameter	A_{ll}	−40.00
Repulsion parameter	$B_{ll} = B_{sl}$	25.00

The particles in many-body DPD simulations interact with pairwise forces. The governing equations of particle motion are given by [36,44]

$$\frac{\mathrm{d}^2\mathbf{r}_\mathrm{i}}{\mathrm{dt}^2} = \sum_{i\neq j}(\mathbf{F}_{ij}^C + \mathbf{F}_{ij}^D + \mathbf{F}_{ij}^R) \tag{1}$$

where $\mathbf{r}_i$ is the position of particle i, and t is the time. $\mathbf{F}_{ij}^C$, $\mathbf{F}_{ij}^D$ and $\mathbf{F}_{ij}^R$ are the conservative, dissipative and random forces experienced by any two particles i and j. The conservative term consists of an attraction and a density-weighted repulsion part:

$$\mathbf{F}_{ij}^C = -A_{\alpha\beta}\omega_C(r_{ij})\mathbf{e}_{ij} + B_{\alpha\beta}(\bar{\rho}_i + \bar{\rho}_j)\omega_d(r_{ij})\mathbf{e}_{ij} \tag{2}$$

where $A_{\alpha\beta} > 0$ is the strength of an attractive force with the interaction range r_c, i.e. $\omega_C(r_{ij}) = (1 - r_{ij}/r_c)$ for $r_{ij} \le r_c$ and $\omega_C(r_{ij}) = 0$ for $r_{ij} > r_c$. Here, $\alpha\beta$ denotes the interaction between liquid (l) particles or solid (s) and liquid (l) particles. $B_{\alpha\beta} > 0$ is the strength of density-weighted repulsive force with the interaction range r_d, i.e. $\omega_d(r_{ij}) = (1 - r_{ij}/r_d)$ for $r_{ij} \le r_d$ and $\omega_d(r_{ij}) = 0$ for $r_{ij} > r_d$. The local density $\bar{\rho}_i$ at the location of particle i is measured by the average $\bar{\rho}_i = \sum_{i\neq j}\omega_\rho(r_{ij})$, where $\omega_\rho = 105/(16\pi r_d^3)(1 + 3r_{ij}/r_d)(1 - r_{ij}/r_d)^3$ for $r_{ij} \le r_d$ and $\omega_\rho = 0$ for $r_{ij} > r_d$. The conservative force between particles is responsible for the thermodynamic behaviour of the system.

The dissipative force is given by

$$\mathbf{F}_{ij}^D = -\gamma\omega_D(r_{ij})(\mathbf{e}_{ij}\cdot\mathbf{v}_{ij})\mathbf{e}_{ij} \tag{3}$$

where γ is the strength of dissipative force and r_{ij} is the distance between particles i and j. $\mathbf{e}_{ij} = (\mathbf{r}_i + \mathbf{r}_j)/r_{ij}$ is the unit vector in the direction from particle j to i. The vector $\mathbf{v}_{ij} = \mathbf{v}_i - \mathbf{v}_j$ is the velocity difference. The weight function is $\omega_d(r_{ij}) = (1 - r_{ij}/r_d)^2$ for $r_{ij} \le r_d$ and $\omega_d(r_{ij}) = 0$ for $r_{ij} > r_d$.

The random force is defined as

$$\mathbf{F}_{ij}^R = \delta\omega_R(r_{ij})\xi_{ij}\Delta t^{-1/2}\mathbf{e}_{ij} \tag{4}$$

where ξ_{ij} is the Gaussian random number with zero mean and unit variance, and δ is the strength of the random force. The relations $\delta = 2\gamma k_BT$ and $\omega_D(r) = [\omega_R(r)]^2$ ensure that the strengths of dissipative and random forces satisfy the fluctuation–dissipation theorem [45,46], where k_B is the Boltzmann constant and T is the temperature of system. Therefore, the dissipative and random forces act effectively as a thermostat that maintains the temperature of system at a specified value. If the system becomes too 'hot', the dissipative force will dominate and cool the system, whereas in too 'cold' system the random forces will dominate and the system temperature will increase. Thus, the specific forms of the dissipative and random forces will define an equilibrium state.

In what follows, we used the DPD units to express all physical quantities, i.e. length in r_c, energy in k_BT and mass in m.

The quantities in Equations (2–4) are taken from the work by Li et al. [34] and they are listed in Table 1. To validate the simulation methods and parameters used in the algorithm, Li et al. [34] compared the simulation results and theoretical predictions of the translation speed of droplet on a substrate with a wettability gradient. It was shown that the simulation results agree well with the theoretical predictions, which indicates the reliability of the simulation model used in the present work. These parameters were also successfully used in other works to study the droplet behaviour on substrate [37,47–49].

The reduced DPD units are directly correlated to the physical units by mapping the density, viscosity, and surface tension of the DPD liquid to the real liquid. Using the same parameters, Lin et al. [49] mapped the liquid in DPD simulations to 80 w/w % glycerol/water solution. The mapping between the physical and DPD units are $l^{physical} = [l] \times l^{DPD}$. Then, the scaling factor, $[l]$, for basic units are $[l] = 6.2349 \times 10^{-5}$m for length, $[l] = 4.8219 \times 10^{-11}$ kg for mass, and$[t] = 7.3322 \times 10^{-5}$s for time. The viscosity and surface tension of the liquid droplet are 4.93 and 7.28 in the DPD units, respectively. The typical velocity of droplet is 0.01, which leads to the Capillary number (the ratio of viscous and surface tension effects), $C_a \approx 6.8 \times 10^{-3}$.

The simulation set-up is presented in Figure 1. It can be seen that the substrate is structured with periodic triangular corrugations. The strength of attractive force between the liquid and wall particles can be used to tailor the wettability of the liquid drop residing on the substrate [34,49]. In our work, the substrate is composed of a superhydrophobic surface (red region in Figure 1) patterned with a hydrophobic stripe (yellow region in Figure 1). Therefore, a sharp wettability step exists at the boundary of the hydrophobic stripe, which is used to guide the motion of the droplet. The density of the substrate is 12. No-slip boundary conditions are enforced by imposing bounce-back reflection condition when liquid particles penetrate into the wall [50]. The substrate is vibrating vertically, i.e. in the y-direction according to $y = a \sin(\omega t)$. The amplitude of the vibration is set as $a = 1.0$. When the substrate is vibrating, the droplet is moving along the stripe as shown in Figure 1, which is consistent with the previous study [21]. The periodic boundary conditions are applied along both the x and z directions. The gravity is also included in our simulations and its magnitude is 8.45×10^{-4} in DPD units. Thus, the typical Bond number (the ratio of the gravity and surface tension) is $B_o \approx 0.28$. A modified velocity-Verlet algorithm [36] is adopted for the numerical integration of the DPD equations with the time step $\Delta t = 0.01$ and the variable factor $\lambda = 0.5$. All simulations were carried out using the open-source MD code, LAMMPS [51].

3. Results and discussion

3.1. Contact angle of droplet at asymmetrically corrugated substrate

In our work, we used the wettability step to guide the droplet motion. Therefore, we first investigate the wetting properties of a droplet in contact with a chemically homogeneous but asymmetrically corrugated substrate. The geometrical features of the substrate are shown in Figure 1. In our set-up, the wettability, measured by the apparent contact angle of droplet, is tuned by changing the magnitude of the attractive force, A_{sl}, between the droplet and substrate particles. To measure the equilibrium apparent contact angle at a given strength of the attractive force, the contour of droplet is obtained from the time-averaged droplet density distribution. Then, the contact angle is measured by fitting the droplet contour near the three-phase contact line using a circle function. Figure 2 shows the apparent contact angle of the droplet the directions perpendicular and parallel to the substrate corrugations. It can be observed in Figure 2 that the contact angle in both directions decreases with increasing A_{sl}. Moreover, the contact angle in the direction perpendicular to the substrate corrugations depends linearly on the magnitude of the attractive force, A_{sl}. Interestingly, this linear dependence is consistent with the results of molecular dynamic simulations where the strength of attractive interaction is controlled by the interaction energy of the Lennard-Jones potential [52].

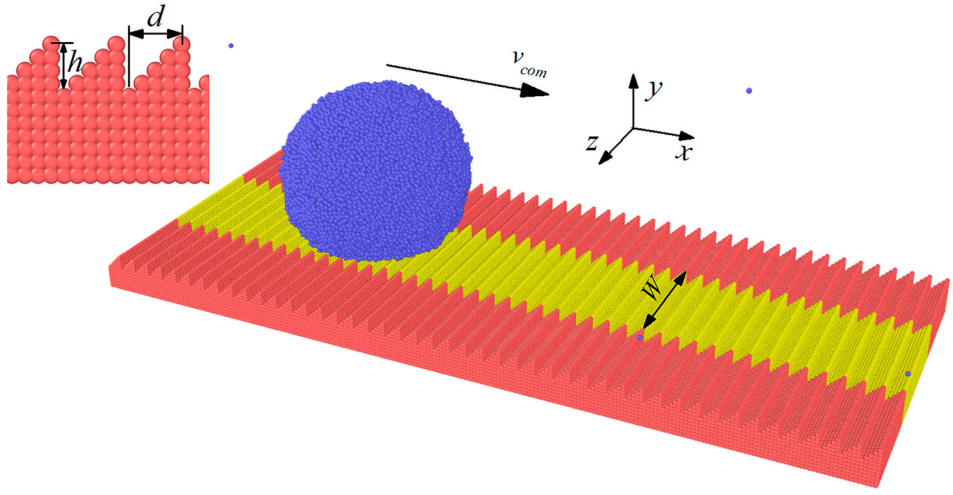

Figure 1. (Colour online) The perspective view of the model. $d = h = 4$ are the width and height of the triangle groove. W is the width of the hydrophobic stripe. The blue spheres denote the liquid droplet. The isolated blue spheres are the vapour atoms of the liquid droplet. The red and yellow spheres are the particles of the superhydrophobic and hydrophobic substrates, respectively.

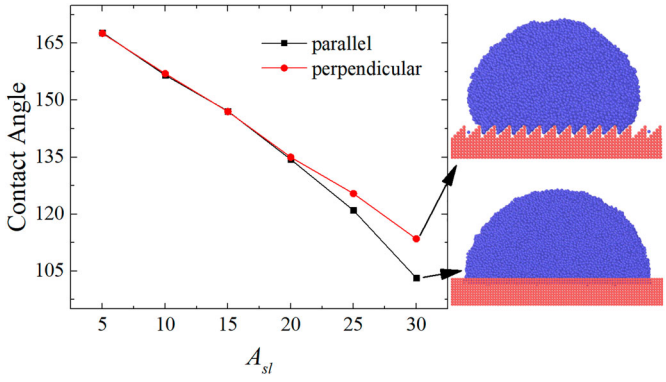

Figure 2. (Colour online) The apparent contact angle of the liquid droplet in contact with chemically homogeneous but asymmetrically corrugated substrate. The up-right and down-right panels are the snapshots of the liquid droplet parallel and perpendicular to asymmetrical grooves when the magnitude of the attractive force is $A_{sl} = 30$ (the rightmost two points in the left panel).

For the weak attractive force between the droplet and substrate particles, i.e. $5 \lesssim A_{sl} \lesssim 20$, surface corrugations do not induce anisotropic wettability. By contrast, for larger attraction force, i.e. $A_{sl} \gtrsim 20$, the droplet preferentially wets the substrate in the direction parallel to the orientation of substrate corrugations. In this case, the apparent contact angle is larger in the direction perpendicular to the substrate corrugations (see Figure 2).

In our study, the wettability step is introduced by the hydrophobic stripe on the superhydrophobic substrate. From Figure 2, the strength of attractive force between the liquid particles and hydrophobic stripe particles is $A_{sl}^{h} = 20$, which corresponds to a value of the contact angle of about 135°. By contrast, the strength of attractive force between the liquid particles and superhydrophobic particles is $A_{sl}^{sh} = 5$, which corresponds to a contact angle of about 167°. As a result, the wettability step with the difference in the apparent contact angle of $\approx 30^{\circ}$ is created to prevent the droplet from moving across the boundaries of the hydrophobic stripe. The demonstration of the proof of concept for the droplet motion along the hydrophobic stripe is presented in the next section.

3.2. Droplet transport along the hydrophobic stripe

In this section, we present the simulation results for the droplet motion on the vibrating substrate by monitoring the position of its centre-of-mass (COM) along the x- and z-directions. Figure 3 shows the time evolution of droplet COM in the x- and z-directions, while the substrate vibrates in the y-direction with the period, $p = 20$. The cases of homogeneous and patterned substrates are compared in order to demonstrate that the presence of a hydrophobic stripe induces a preferential direction of motion on a vibrated substrate. It can be seen in Figure 3 that the x-component of the COM increases with time for homogeneous and patterned substrates, indicating that the substrate vibration induces droplet motion in the $+x$-direction. It can be further noticed that the time evolution of the x-component of COM is not represented by smooth and monotonic lines, suggesting that the instantaneous velocity of the droplet is not a constant. The mechanism of droplet motion, induced by vibration of an asymmetrically corrugated substrate, was examined by Tretyakov and Müller [21]. It was shown that as the substrate moves upwards, it pushes the droplet and forces it to move to left ($-x$-direction). When the substrate moves downwards, the substrate pulls the droplet and the droplet tends to move right ($+x$-direction). During a vibration period, the pulling effect is greater than the pushing effect, which leads to the net droplet motion in the $+x$-direction.

As shown in Figure 3, in the absence of the hydrophobic stripe, the z-component of COM oscillates widely around the initial position, namely, the droplet moves irregularly along the z-direction as it is transported along the $+x$-direction. In contrast, for the substrate patterned with a hydrophobic stripe, the z-component of droplet COM oscillates around the initial value with a small amplitude. The apparent oscillation of the z-component occurs because the width of hydrophobic stripe is larger than that of droplet in contact with the substrate, which results in periodic motion of the droplet from one edge of the stripe to another. The oscillation of the COM z-component indicates that the wettability step at the edge of hydrophobic stripe prevents the droplet motion along the z-direction. The results in Figure 3 demonstrate that the presence of a hydrophobic stripe on an asymmetrically corrugated, superhydrophobic substrate induces unidirectional motion of the droplet when the substrate is vibrated, while in the absence of the stripe, the droplet motion becomes irregular. It can be further noticed in Figure 3 that the instantaneous x-component of COM is larger for the substrate with a hydrophobic stripe than without the stripe, i.e. larger average velocity of the droplet on the substrate with a hydrophobic stripe.

3.3. The droplet velocity along the hydrophobic stripe

In the previous section, we demonstrated the feasibility of the droplet motion along a hydrophobic stripe using a vibrating

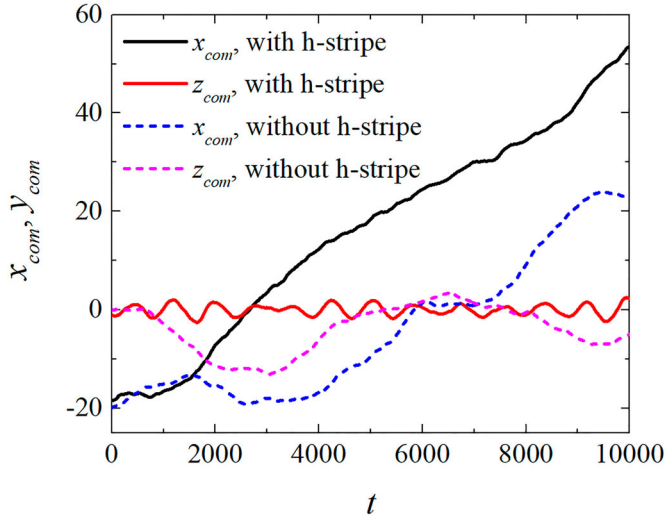

Figure 3. (Colour online) The time evolution of centre-of-mass of the droplet in the x- and z-directions, while the droplet is transported in the x-direction. The period of substrate vibration, $p = 20$. The diameter of the droplet is $D \approx 20$. The notations 'with h-stripe' and 'without h-stripe' indicate that the substrate is patterned with a hydrophobic stripe and homogeneous, respectively. The width of hydrophobic stripe is $W = 20$.

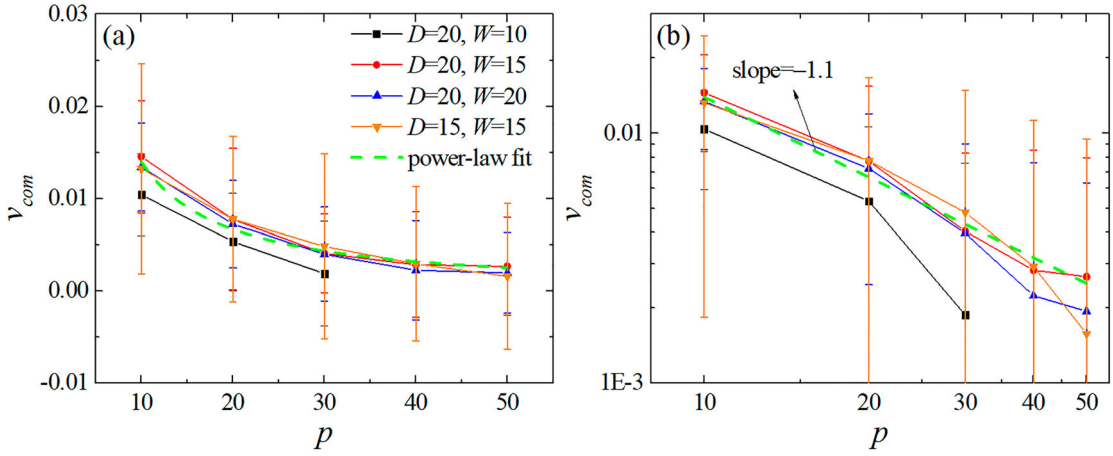

Figure 4. (Colour online) (a) The time-averaged velocity of the centre-of-mass of droplets, v_{com} vs. the period of substrate vibration, p for different droplet sizes, D, and the stripe widths, W. The error bars represent the standard deviation of the instantaneous velocity of the centre-of-mass during the time interval of 10^4. The dashed green line is a power-law fitting. (b) The same data replotted on the log–log scale.

substrate patterned with asymmetric corrugations. In this section, we investigate the dependence of velocity of the droplet COM on the droplet diameter, the period of substrate vibration, and the width of the hydrophobic stripe. The results are shown in Figure 4. We considered two values of the droplet diameter $D \approx 20$ and 15. The hydrophobic stripe width is $W = 10$, 15 and 20 for $D \approx 20$, while for the droplet size $D \approx 15$, the stripe width is $W = 15$. The period of the substrate vibration varies from $p = 10$ to 50. It can be seen in Figure 4 that the velocity of the droplet COM decreases with increasing vibration period, which is consistent with the results of the previous MD study [21]. The velocity of the droplet is determined by the energy input per unit time injected into the droplet due to the substrate vibration. The input energy per unit time, i.e. input power, P_{in}, can be expressed as [21]

$$P_{in} = \frac{1}{p}\int_0^p v_y^s F^s(t) \cdot n_y dt \tag{5}$$

where $v_y^s(t)$ and $F^s(t)$ are the velocity of the substrate and the total force exerted by the substrate on the droplet, respectively. The velocity of the substrate, $v_y^s(t) \sim \frac{1}{p}$, decreases as the period of the substrate vibration increases, leading to a reduced COM velocity. Moreover, P_{in} is proportional to the contact area (A) between the droplet and the substrate because $F^s(t)$ scales with the number of solid–liquid interactions. The value of A can be measured by the area in the xz-plane within the three-phase contact line. As the width of the hydrophobic stripe increases from $W = 10$ to $W = 15$ for $D \approx 20$, the contact area increases from $A \approx 78$ to $A \approx 176$, resulting in larger input power, consequently, larger velocity of the droplet. For the case $W = 10$, the velocity of COM is too small to be identified accurately in our simulations for the vibration periods $p = 40$ and 50 (see Figure 4). When the width of the hydrophobic stripe increases from 15 to 20, A remains the same. As a consequence, the velocity of droplet COM is unchanged for the droplet diameter, $D \approx 20$, as shown in Figure 4.

For the droplet diameter $D \approx 20$ with the hydrophobic stripe width, $W = 20$, and the diameter $D \approx 15$ with the stripe width $W = 15$, the velocity of droplet COM is nearly the same for a given period of substrate vibration. The range of vibration periods considered in our study corresponds to the large vibration period regime reported in the previous study [21]. In the large vibration period regime, the ratio, P_{in}/A, does not depend on the droplet diameter, which leads to the same droplet velocity regardless of the droplet size. It is interesting to note that the relationship between the velocity of COM

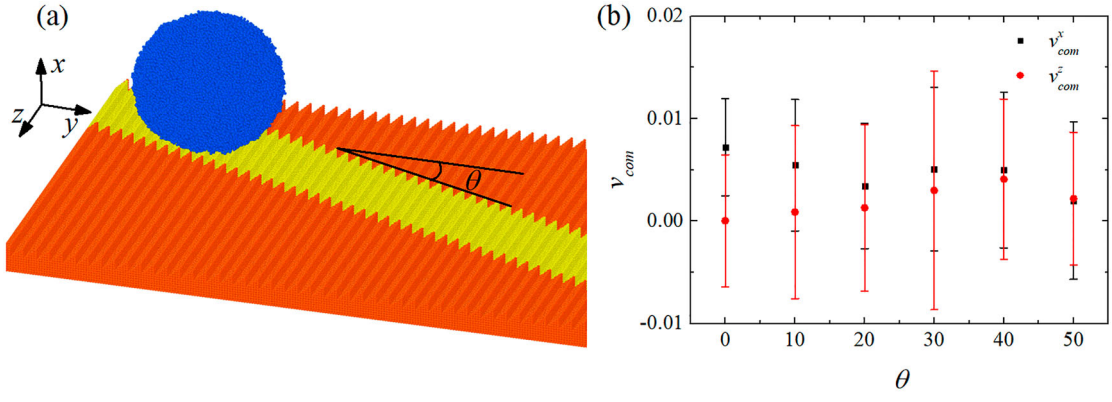

Figure 5. (Colour online) (a) The three-dimensional view of the simulation model. The angle θ is used to denote the orientation of the hydrophobic stripe. (b) The velocity of droplet centre-of- mass, v_{com}, for different θ. The error bars are the standard deviation of v_{com} during the time interval of 10^4.

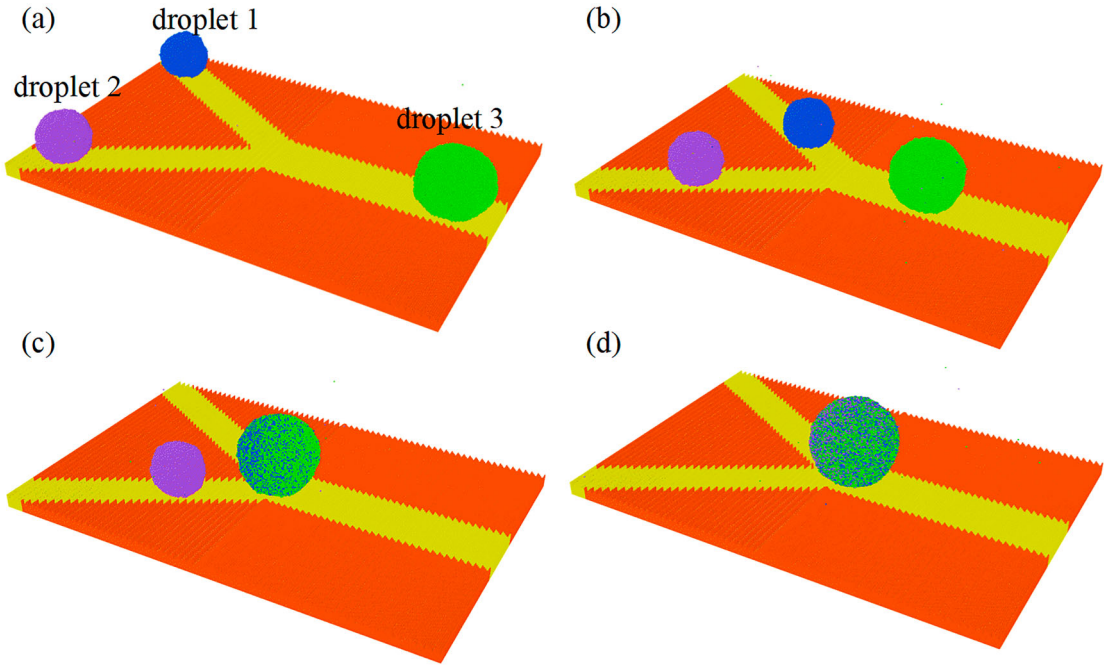

Figure 6. (Colour online) A series of consecutive snapshots of three droplets with different initial locations moving towards the centre of the substrate and coalescing with each other at the intersection.

and the period of substrate vibration can be well described by the power-law function, $v_{\mathrm{com}} \sim p^b$ with $b \approx -1.1$ (see Figure 4). A similar power-law dependence between the input power per contact area and the vibration period can be obtained from the data reported in the previous study [21]. Moreover, the power-law exponent, $b \approx -1.2$, in the previous study is consistent with the fitting value in our work. The underlying mechanism of the power-law dependence will be clarified in the future.

Next, we examine the velocity of droplet COM for different orientations of the hydrophobic stripe with respect to the surface corrugations. The hydrophobic stripe orientation is defined by the angle, θ, shown in Figure 5(a). The diameter of the droplet is $D \approx 20$ and the period of substrate vibration is $p = 20$. It can be seen in Figure 5 that the velocity of COM remains nearly unchanged as the orientation of the hydrophobic stripe, θ, increases from 0° to 50°. It should be commented that this is a useful feature of our droplet transportation strategy, since the change in the orientation of the hydrophobic stripe does not significantly slow down droplet motion.

3.4. Continuous transport of multiple droplets

The advantage of the proposed strategy is that the direction of droplet motion can be controlled by the orientation of the hydrophobic stripe and asymmetric corrugation of the substrate. In this section, we demonstrate that multiple droplets with different initial locations can be transported towards the same location and coalesce into large droplets. Figure 6 illustrates a series of snapshots of three droplets initially located at different positions on the substrate and transported to the intersection. The mirror-symmetric corrugation of substrate is constructed as triangle shapes with the normal vector of hypotenuse pointing to left (right) in the left (right) side of the substrate (see Figure 6). Three hydrophobic stripes form a 'Y' shape track (see Figure 6). The width of the two branches is 15, and the angle between the two branches of the 'Y' track is 60°. The width of the horizontal hydrophobic stripe is 20. The droplets 1 and 2 are initially located at the up-left and down-left sides of the substrate. The diameter of droplets 1 and 2 is $D \approx 15$. A relatively large droplet with diameter, $D \approx 20$, is initially located on the mid-right of the substrate. Forced by the substrate vibration, three droplets simultaneously move towards the centre of the substrate, as shown in Figure 6(b). Due to fluctuation of the initial COM velocities, the droplets 1 and 3 first come in contact with each other and coalesce into one large droplet at the centre of the substrate, as shown in Figure 6(c). Then, the droplet 2 joins the coalesced droplet and, finally, all droplets coalesce into the large droplet (Figure 6(d)). As the mixing proceeds, the substrate continuously vibrates to enhance the mixing rate without allowing the coalesced droplet to move to another location. As is evident from Figure 6(d), the fluid particles from the three droplets become thoroughly mixed inside the coalesced droplet.

The direct droplet transport method enables generation of continuous motion of the droplet. The amplitude of the substrate vibration is small (10 μm), leading to insignificant vibration of the whole platform. By combining the asymmetric corrugations and patterned wettability on a vibrating substrate, multiple droplets can be transported to the same location. The asymmetric corrugations and patterned wettability can be manufactured outside cleanrooms and operated without special equipment. Such method can be used to transport droplets in affordable, open-channel microfluidic devices for various applications. To efficiently transport the droplet, the frequency of substrate vibration needs to be relatively high, which may

restrict applications in certain cases where vibration should be avoided.

4. Conclusion

We proposed a novel strategy to generate directed droplet motion along a hydrophobic stripe using periodic vibration of a substrate with asymmetric corrugations. Using many-body dissipative particle dynamic (DPD) simulations, we first investigated the static wetting properties of a liquid droplet on an asymmetrically corrugated, homogeneous substrate. We find that the dependence of the apparent contact angle on the attractive interaction parameter between liquid and solid particles is well described by a linear function. Moreover, a spatial variation of the interaction parameter can lead to a large wettability step on the substrate, which effectively restricts the motion a liquid droplet within a stripe. We further demonstrated that the asymmetric, triangle corrugation of a vibrated substrate induces droplet motion, while the wettability contrast along the stripe determines the direction of its motion. In addition, we found that the droplet velocity increases with decreasing substrate vibration period, but it is nearly independent of the droplet size and hydrophobic stripe orientation. A power-law dependence between the droplet velocity and the vibration period was also identified. Using our strategy, we showed that multiple droplets at different initial locations can be transported along intersecting hydrophobic stripes towards a single spot for mixing. The numerical results obtained in this work open the possibility for the design of efficient methods for the vibration-induced droplet transport in DMF devices.

Acknowledgements

Computational work in support of this research was performed at the National Supercomputer Centre in Tianjin, China.

Disclosure statement

No potential conflict of interest was reported by the authors.

Funding

This work was supported by the National Natural Science Foundation of China [grant number 21606099].

References

[1] Squires TM, Quake SR. Microfluidics: fluid physics at the nanoliter scale. Rev Mod Phys. 2005;77(3):977–1026.
[2] Samiei E, Tabrizian M, Hoorfar M. A review of digital microfluidics as portable platforms for lab-on a-chip applications. Lab Chip. 2016;16(13):2376–2396.
[3] Lapierre F, Jonsson-Niedziolka M, Coffinier Y, et al. Droplet transport by electrowetting: lets get rough. Microfluid Nanofluid. 2013;15(3):327–336.
[4] Cui WW, Zhang ML, Duan XX, et al. Dynamics of electrowetting droplet motion in digital Microfluidics systems: from dynamic saturation to device physics. Micromachines. 2015;6(6):778–789.
[5] Raman KA, Jaiman RK, Lee TS, et al. A numerical study on electrowetting-induced jumping and transport of droplet. Int J Heat Mass Tran. 2016;99:805–821.
[6] Aminfar H, Mohammadpourfard M. Droplets merging and stabilization by electrowetting: Lattice Boltzmann study. J Adhes Sci Technol. 2012;26(12–17):1853–1871.
[7] Yeh S-I, Fang W-F, Sheen H-J, et al. Droplets coalescence and mixing with identical and distinct surface tension on a wettability gradient surface. Microfluid Nanofluid. 2013;14(5):785–795.
[8] Bansal S, Sen P. Effect of electrowetting induced capillary oscillations on coalescence of compound droplets. J Colloid Interf Sci. 2018;530:223–232.
[9] Mugele F, Baret JC, Steinhauser D. Microfluidic mixing through electrowetting-induced droplet oscillations. Appl Phys Lett. 2006;88(20):204106.
[10] Lai Y-H, Hsu M-H, Yang J-T. Enhanced mixing of droplets during coalescence on a surface with a wettability gradient. Lab Chip. 2010;10(22):3149–3156.
[11] Guan Y, Tong AY. A numerical study of droplet splitting and merging in a parallel-plate electrowetting-on-dielectric Device. J Heat Trans T Asme. 2015;137(9):091016.
[12] Choi S, Kwon Y, Choi Y-S, et al. Improvement in the breakdown properties of electrowetting using polyelectrolyte ionic solution. Langmuir. 2013;29(1):501–509.
[13] Mibus M, Jensen C, Hu X, et al. Dielectric breakdown and failure of anodic aluminum oxide films for electrowetting systems. J Appl Phys. 2013;114(1):014901.
[14] Morrissette JM, Mahapatra PS, Ghosh A, et al. Rapid, self-driven liquid mixing on open-surface microfluidic platforms. Sci Rep-UK. 2017;7(1):1800.
[15] Pratap V, Moumen N, Subramanian RS. Thermocapillary motion of a liquid drop on a horizontal solid surface. Langmuir. 2008;24(9):5185–5193.
[16] Bjelobrk N, Girard H-L, Bengaluru Subramanyam S, et al. Thermocapillary motion on lubricant-impregnated surfaces. Phys Rev Fluids. 2016;1(6):063902.
[17] Dai Q, Khonsari MM, Shen C, et al. Thermocapillary migration of liquid droplets induced by a unidirectional thermal gradient. Langmuir. 2016;32(30):7485–7492.
[18] Suda H, Yamada S. Force measurements for the movement of a water drop on a surface with a surface tension gradient. Langmuir. 2003;19(3):529–531.
[19] Moumen N, Subramanian RS, McLaughlin JB. Experiments on the motion of drops on a horizontal solid surface due to a wettability gradient. Langmuir. 2006;22(6):2682–2690.
[20] Chowdhury IU, Sinha Mahapatra P, Sen AK. Self-driven droplet transport: effect of wettability gradient and confinement. Phys Fluids. 2019;31(4):042111.
[21] Tretyakov N, Muller M. Directed transport of polymer drops on vibrating superhydrophobic substrates: a molecular dynamics study. Soft Matter. 2014;10(24):4373–4386.
[22] Hu Q, Ren Y, Liu W, et al. Fluid flow and mixing induced by AC continuous electrowetting of liquid metal droplet. Micromachines. 2017;8(4):119.
[23] Wang JD, Chen S, Chen DR. Spontaneous transition of a water droplet from the Wenzel state to the Cassie state: a molecular dynamics simulation study. Phys Chem Chem Phys. 2015;17(45):30533–30539.
[24] Gao S, Liao QW, Liu W, et al. Effects of solid fraction on droplet wetting and vapor condensation: a molecular dynamic simulation study. Langmuir. 2017;33(43):12379–12388.
[25] Ambrosia MS, Ha MY. A molecular dynamics study of Wenzel state water droplets on anisotropic surfaces. Comput Fluids. 2018;163:1–6.
[26] Li H, Yan TY, Fichthorn KA, et al. Dynamic contact angles and mechanisms of motion of water droplets moving on nanopillared

superhydrophobic surfaces: a molecular dynamics simulation study. Langmuir. 2018;34(34):9917–9926.
[27] Drazer G, Khusid B, Koplik J, et al. Wetting and particle adsorption in nanoflows. Phys Fluids. 2005;17(1):017102.
[28] Moosavi A, Rauscher M, Dietrich S. Size dependent motion of nano-droplets on chemical steps. J Chem Phys. 2008;129(4):044706.
[29] Rauscher M, Dietrich S. Nano-droplets on structured substrates. Soft Matter. 2009;5(16):2997–3001.
[30] Zhang Z, Zhao CR, Yang XT, et al. Micrometer-sized droplet impingement dynamics on flat and micro-structured surfaces. Ann Nucl Energy. 2018;112:464–473.
[31] Wang X, Sun D-L, Wang X-D, et al. Dynamics of droplets impacting hydrophilic surfaces decorated with a hydrophobic strip. Int J Heat Mass Transf. 2019;135:235–246.
[32] Ding H, Spelt PDM. Inertial effects in droplet spreading: a comparison between diffuse-interface and level-set simulations. J Fluid Mech. 2007;576:287–296.
[33] Li S, Fan H. On multiscale moving contact line theory. P Roy Soc A Math Phy. 2015;471(2179):20150224.
[34] Li Z, Hu GH, Wang ZL, et al. Three dimensional flow structures in a moving droplet on substrate: a dissipative particle dynamics study. Phys Fluids. 2013;25(7):072103.
[35] Li Z, Drazer G. Hydrodynamic interactions in dissipative particle dynamics. Phys Fluids. 2008;20(10):103601.
[36] Espanol P, Warren PB. Perspective: dissipative particle dynamics. J Chem Phys. 2017;146(15):150901.
[37] Warren PB. Vapor-liquid coexistence in many-body dissipative particle dynamics. Phys Rev E. 2003;68(6):066702.
[38] Wang Y, Chen S. Droplets impact on textured surfaces: mesoscopic simulation of spreading dynamics. Appl Surf Sci. 2015;327:159–167.
[39] Zhao J, Chen S, Liu Y. Dynamical behaviors of droplet impingement and spreading on chemically heterogeneous surfaces. Appl Surf Sci. 2016;400:515–523.
[40] Zhao J, Chen S, Liu Y. Droplets motion on chemically/topographically heterogeneous surfaces. Mol Simulat. 2016;42(17):1452–1459.
[41] Wang L, Rui Z, Zhang X, et al. Numerical simulation of droplet impact on textured surfaces in a hybrid state. Microfluid Nanofluid. 2017;21(4):61.
[42] Zhao JY, Chen S. Following or against topographic wettability gradient: movements of droplets on a micropatterned surface. Langmuir. 2017;33(21):5328–5335.
[43] Zhang K, Chen S, Wang Y. Ratio dependence of contact angle for droplet wetting on chemically heterogeneous substrates. Colloid Surface A. 2018;539:237–242.
[44] Groot RD, Warren PB. Dissipative particle dynamics: bridging the gap between atomistic and mesoscopic simulation. J Chem Phys. 1997;107(11):4423–4435.
[45] Hoogerbrugge PJ, Koelman J. Simulating microscopic hydrodynamic phenomena with dissipative particle dynamics. Europhys Lett. 1992;19(3):155–160.
[46] Espanol P, Warren P. Statistical-mechanics of dissipative particle dynamics. Europhys Lett. 1995;30(4):191–196.
[47] Merabia S, Pagonabarraga I. A mesoscopic model for (de)wetting. Eur Phys J E. 2006;20(2):209–214.
[48] Cupelli C, Henrich B, Glatzel T, et al. Dynamic capillary wetting studied with dissipative particle dynamics. New J Phys. 2008;10(4):043009.
[49] Lin CS, Chen S, Xiao LL, et al. Tuning drop motion by chemical chessboard-patterned surfaces: a many-body dissipative particle dynamics study. Langmuir. 2018;34(8):2708–2715.
[50] Revenga M, Zúñiga I, Español P, et al. Boundary models in DPD. Int J Modern Phys C. 1998;09(08):1319–1328.
[51] Plimpton S. Fast parallel algorithms for short-range molecular-dynamics. J Comput Phys. 1995;117(1):1–19.
[52] Sendner C, Horinek D, Bocquet L, et al. Interfacial water at hydrophobic and hydrophilic surfaces: slip, viscosity, and diffusion. Langmuir. 2009;25(18):10768–10781.